Journal of Magnetism and Magnetic Materials 323 (2011) 767–774

Contents lists available at ScienceDirect

Journal of Magnetism and Magnetic Materials

journal homepage: www.elsevier.com/locate/jmmm

Magnetic properties of nanoparticles useful for SQUID relaxometry in biomedical applications

H.C. Bryant [a,c,*], Natalie L. Adolphi [a,d], Dale L. Huber [b], Danielle L. Fegan [a], Todd C. Monson [b], Trace E. Tessier [a], Edward R. Flynn [a]

[a] Senior Scientific LLC, 11109 Country Club NE, Albuquerque, NM 87111, USA
[b] Sandia National Laboratories, P.O. Box 5800, Albuquerque, NM 87185, USA
[c] Department of Physics and Astronomy, University of New Mexico, Albuquerque, NM 87131, USA
[d] Department of Biochemistry and Molecular Biology, University of New Mexico, Albuquerque, NM 87131, USA

ARTICLE INFO

Article history:
Received 1 April 2010
Received in revised form
7 October 2010
Available online 3 November 2010

Keywords:
Magnetic nanoparticle
AC susceptometry
Magnetorelaxometry
Langevin function
Néel relaxation
Magnetite

ABSTRACT

We use dynamic susceptometry measurements to extract semiempirical temperature-dependent, 255–400 K, magnetic parameters that determine the behavior of single-core nanoparticles useful for SQUID relaxometry in biomedical applications. Volume susceptibility measurements were made in 5 K degree steps at nine frequencies in the 0.1–1000 Hz range, with a 0.2 mT amplitude probe field. The saturation magnetization (M_s) and anisotropy energy density (K) derived from the fitting of theoretical susceptibility to the measurements both increase with decreasing temperature; good agreement between the parameter values derived separately from the real and imaginary components is obtained. Characterization of the Néel relaxation time indicates that the conventional prefactor, 0.1 ns, is an upper limit, strongly correlated with the anisotropy energy density. This prefactor decreases substantially for lower temperatures as K increases. We find, using the values of the parameters determined from the real part of the susceptibility measurements at 300 K, that SQUID relaxometry measurements of relaxation and excitation curves on the same sample are well described.

1. Introduction

Magnetic nanoparticles show much promise in labeling cancer cells or other pathological structures, which may then be detected by SQUID (Superconducting Quantum Interference Device) relaxometry. The critical magnetic properties for this application are relaxation times and spontaneous magnetization.

In order to label biological structures magnetically for detection by SQUID relaxometry, the nanoparticles with their coatings of specific antibodies must be undetectable when not firmly attached to the target object; i.e., when the particles of interest are free to reorient in their suspending fluid, they should have relaxation times much shorter than the observation time; however, if rotation of the nanocrystal is hindered by its attachment through antibody–antigen interactions with the target structure, the relaxation time can be comparable to the SQUID observation time, typically of the order of a second [1]. In the former case, the relaxation time for rotation in a fluid is very short for hydrodynamic radii typical of the particles considered, rendering them invisible to the SQUID system. In the latter case, when rotation of the crystal lattice of the particle is hindered, the magnetic moment of the single domain nanocrystal, typically a few hundred thousand Bohr magnetons in magnetite, reorients with characteristic relaxation times first discussed by Néel [2]. The Néel time is of critical importance because its exponential dependence on particle volume severely limits the sizes of the particles that are suitable for SQUID relaxometry. As we shall see below, the "SQUID window", the material-dependent size range for which SQUIDs can sense decaying magnetism from relaxing nanoparticles, is about only 2 nm wide centered on a diameter of 26 nm at room temperature, for the magnetite particles discussed here.

In our analysis we do not consider interactions among nanoparticles [3] although we modify the Langevin function to reflect the disorienting effects of anisotropy with a random easy axis distribution of an ensemble of fixed particles.

After briefly discussing the theoretical models, we compare the fitting of our predictions to results of a susceptibility study of the nanoparticle properties from 255 to 400 K. We then report observations of these same particles under SQUID relaxometry, at room temperature and three different magnetic field pulse durations, comparing with predictions from the parameters determined from the dynamic susceptibility analysis. We shall use SI units throughout.

* Corresponding author at: Senior Scientific LLC, 11109 Country Club NE, Albuquerque, NM 87111, USA. Tel.: +1 505 243 1058.
E-mail address: hzero@unm.edu (H.C. Bryant).

0304-8853/$ - see front matter © 2010 Elsevier B.V. All rights reserved.
doi:10.1016/j.jmmm.2010.10.042

2. Material and methods

2.1. Nanoparticles

The nanoparticles discussed in this paper were supplied by Ocean NanoTech (Springdale AR, USA), designated as Ocean SHP 30 lot DE4G. These magnetite particles were suspended in water with an iron content measured by the phenanthroline assay to be 28.8 mg [Fe]/ml. 10 μl of suspension was pipetted onto a cotton swab "Q Tip" (Unilever, Trumbull, CT, USA), and allowed to dry in zero applied field. We assume the particles are firmly attached to the cotton fibers so that the crystal lattices themselves cannot rotate in response to an applied field. This cotton swab was our primary sample for the measurements reported in this paper. Since Fe_3O_4 is 0.7235 Fe by weight, we find the mass of magnetite nanoparticles in the sample to be 398 μg. From TEM images (Tecnai G^2 F30 at 300 kV, FEI Corporation, Hillsboro, OR, USA), a distribution of Feret[1] diameters of the particles was determined using the program ImageJ (produced through an NIH grant and available on the internet). The distribution peaked at 25 nm with a full width at half maximum (FWHM) of 4 nm.

2.2. Susceptometry

We determined the induced magnetic moment of the Q Tip sample at 9 frequencies and 30 temperatures, using an MPMS-7 SQUID magnetometer (Quantum Design, San Diego, CA, USA), with a palladium reference sample for calibration. The software associated with the apparatus presents the magnetic moment results in emu (erg/G). These numbers are converted to volume susceptibility in the emu system by dividing the magnetic moment by the amplitude of the driving field (2 Oe) and by the total volume of the magnetite, 7.56×10^{-5} cm^3 (398 μg at a density of 5.24 g/cm^3) in the sample. We converted the resulting (dimensionless emu) volume susceptibilities into (dimensionless rationalized MKS) volume susceptibilities by multiplying the former by 4π.

2.3. SQUID relaxometry

The SQUID relaxometry measurement technique and the apparatus used for the measurements reported here have been described in detail elsewhere [4,5]. Briefly, the nanoparticle sample is magnetized using an applied DC magnetic field pulse ranging from 0 to 4 mT in amplitude and from 0.3 to 1.5 s in duration. Beginning at 50 ms after the end of the field pulse, the decaying sample magnetization is measured for 2 s using a 7-channel SQUID array.

3. Theoretical model

3.1. Néel relaxation, anisotropy and field effects

Néel relaxation is principally governed by the coupling energy of the collective electron spin with special directions in the crystal lattice. This anisotropy energy can also have contributions from the morphology of the nanoparticle such as shape and surface anisotropy [6]. Configurational anisotropy has been studied in single and pseudo-single domain grains of magnetite and the effects are comparable to magnetocrystalline anisotropy [7]. In the treatment below, we shall include, as is commonly done in this field, the anisotropy energy density in a single parameter K (J/m^3), and treat magnetite as a uniaxial crystal, ignoring the fact that its magnetocrystalline anisotropy is triaxial (cubic) [8]. This approach to understanding the particle is therefore semiempirical in an attempt to restrict parameters to as few as possible for a reasonable description of the magnetic behavior for biomedical applications.

The Néel relaxation time is affected by strength of the applied magnetic field. We shall represent the relaxation time [5,9] in the presence of an applied field by

$$\tau_N = \tau_0 \exp(Kv\beta/kT), \tag{1}$$

where v is the particle volume, $\beta=(1-B/B_K)^{\alpha}$ and $B_K=2\ K/M_s$ the switching field. For the relaxometry data we use $\alpha=3/2$, consistent with the theoretical work of Victora [10]. M_s, B, k and T are the spontaneous magnetization (J/Tm^2), applied field (Tesla), Boltzmann's constant (1.38×10^{-23} J/K) and absolute temperature (K), respectively. For susceptibility measurements (Section 4) the field-reduction in time constant is negligible, but it must be taken into account for relaxometry measurements (Section 5), which require much higher fields (4 mT).

In our modeling, we leave τ_0, treated solely as a function of temperature, to be fit with the susceptibility data (Section 4).

3.2. The modified Langevin function

The equilibrium polar angle θ of alignment of a dipole with an applied field is determined by the balance between the torque exerted on the dipole by the field and the disorienting effect of thermal fluctuations. When these two effects are the only agents present, the average value of $\cos\theta$ is the Langevin function L [10].

However, when the dipole is a single domain nanoparticle, fixed so the crystal cannot rotate, anisotropy can hinder alignment with the external field. In this case the particle energy used in deriving the Langevin function may be replaced by

$$U = -M_s v B\hat{e}\hat{b} - Kv(\hat{e}\hat{n})^2, \tag{2}$$

to form a distribution function including anisotropy [11,12], where the unit vectors, $\hat{e}$, $\hat{b}$ *and* $\hat{n}$, denote the directions of the magnetic moment, the applied field and the anisotropy axis, respectively,

$$W(\hat{e}) = \exp(-U/kT)/Z, \tag{3}$$

where $Z(\sigma,\xi) = \int \exp(-U/kT)d\hat{e}$, with $\sigma=Kv/kT$ and $\xi=M_svB/kT$.

The expectation value of orientation of the magnetic moment with the applied field B is then given by

$$<\hat{e}\hat{b}> = \int \hat{e}\hat{b}W(\sigma,\xi)d\hat{e}. \tag{4}$$

We shall refer to this expression as the "modified Langevin function" for which, the Langevin function L is the limiting case when $\sigma=0$.

The distribution function plays different roles in the susceptibility and relaxometry measurements. The modified Langevin function may be numerically computed using a formula derived by Yasumori et al. [13] for an isotropic distribution of fixed anisotropy axes. The ratio of the modified L to L, displayed in Fig. 1 in a form useful in modeling our data, is consistent numerically with Fig. 1 of Bentivegna et al. [14].

3.3. Dynamic susceptibility model

Raikher and Stepanov [12] have treated the theory of dynamic susceptibility of nanoparticles; we refer the reader to their discussion and insights, starting with the distribution function $W(\hat{e})$ defined above. In the susceptibility case, the alignment of the particle's magnetic moment with applied B can be treated as a perturbation to its energy U (Eq. (2)). Their Eq. (40) gives the real

[1] The Feret diameter is the largest caliper measurement that can be made on the TEM image of the particle. A caliper measurement is the distance between two parallel planes each just touching the surface of the object.

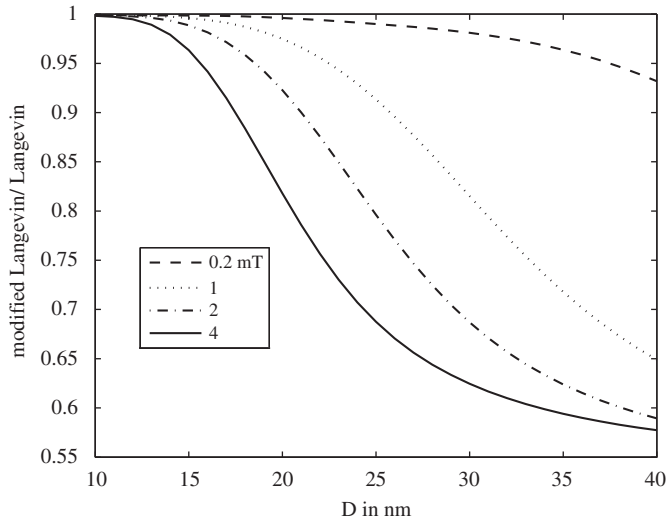

Fig. 1. Ratio of the modified Langevin to the usual Langevin function plotted vs. a range of spherical nanoparticle diameters and applied fields discussed in this paper. Bulk properties of magnetite at 300 K are used: $K=1.35\times10^4$ J/m^3 and $M_s=4.72\times10^5$ J/Tm^3.

and imaginary, linear, dynamic susceptibilities for hindered nanoparticles (assumed uniformly spherical of diameter D and volume v, with randomly frozen anisotropy axes), leading in our case to

$$\chi' = \frac{\mu_0}{9kT} N M_s^2 \int_0^\infty \left[3+2(1-S_2)(\omega\tau_{10})^2\right] \frac{v^2 w(D) dD}{1+(\omega\tau_{10})^2} \tag{5}$$

and

$$\chi'' = \frac{\mu_0}{9kT} N M_s^2 \int_0^\infty (1+2S_2) \frac{\omega\tau_{10} v^2 w(D) dD}{1+(\omega\tau_{10})^2} \tag{6}$$

where

$$S_2 = \frac{1}{2}\int_{-1}^{1}(3y^2-1)\exp(\sigma y^2)dy \Big/ \int_{-1}^{1}\exp(\sigma y^2)dy \tag{7}$$

For large σ, $S_2 \cong 1-3/2\sigma$, [12] although we used the numerical integration (Eq.(7)) to allow for any unexpected small values of σ.

The relaxation time, based on the work of Bessais et al. [15] as suggested by Raikher and Stepanov [12] is

$$\tau_{10} = \tau_0 \sigma (1+\sigma/4)^{-5/2} \exp(\sigma\beta), \tag{8}$$

is a modification of Eq. (1). N is the number of nanoparticles per unit volume, given by the reciprocal of mean volume, discussed below, derived from the measured distribution of particle diameters, $w(D)$.

3.4. Moment observed by relaxometry

In relaxometry, a relatively strong DC magnetic pulse is applied to the nanoparticle sample, and the subsequent collective magnetic moment is measured as a function of time after the pulse is switched off. Here we describe the response using a modification of the Moment Superposition Model (MSM) [16–18]. The observed induced magnetic moment and its subsequent decay arise from the mechanisms presented below. A square pulse of strength B is applied for a time t_p, and the magnetic moment $M(t)$ of the sample is given at time t after the pulse is turned off:

$$M(t) = n\int_0^\infty \mu L(\sigma,\xi) w(D) g(t_p) \exp(-t/\tau) dD, \tag{9}$$

where n is the number of particles in the sample, $\mu=vM_s$ the magnetic moment of a particle of diameter D and $L(\sigma,\ \xi)$ the modified Langevin function discussed above (Section 3.2). The "Néel factor" is given by $g(t_p)=1-\exp(-t_p/\tau_N)$, and τ is just τ_N with the applied field of $\beta=1$. We replace τ_0 with $\tau_0\sigma(1+\sigma/4)^{-5/2}$, consistent with Eq. (8)

4. Susceptibility measurements

4.1. Size distribution

Fig. 2 displays the distribution of Feret diameters of the sample measured by TEM, about 2600 particles. A sub-sample of these particles was analyzed by the program ImageJ. There is evidence that the particles tend to be less round as the Feret diameter increases between 20 and 30 nm. Although we assume spherical particles in our models, the circularity (4π *area/perimerter*^{2}), for example, for a Feret diameter of 25 nm in our sample is around 0.77. For a circle it is 1.

4.2. Number density

Using the measured probability distribution $w(D)$ of Feret diameters (Fig. 2) and ignoring any departure from sphericity, we find the average particle volume in our sample:

$$\overline{v} = \int_0^\infty w(D) v dD = 8.1x10^{-24}\text{m}^3. \tag{10}$$

From the total volume of magnetite in the sample (Section 2.2), we estimate the number of nanoparticles on the cotton swab sample as $n=9.4\times10^{12}$. We take the volume V of the sample to be just the total volume of the particles themselves, so that $V=n\overline{v}$. Consequently, the number density N in Eqs.(5) and (6) reduces to $1/\overline{v}$, and n does not enter into our model even though it determines the strength of the total dipole moment measured by the magnetometer.

4.3. Comparison with model

The model for susceptibility was fitted to the measurements, Fig. 3a and b, by adjusting the values of the three temperature-dependent parameters (K, M_S, τ_0) to minimize the rms differences between the modeled and measured quantities, for each of the 30 temperatures for which the real and imaginary susceptibilities were measured. In our fitting we ignored the possibility that these three parameters could depend on particle size. The real and imaginary parts were treated separately and the outcomes can

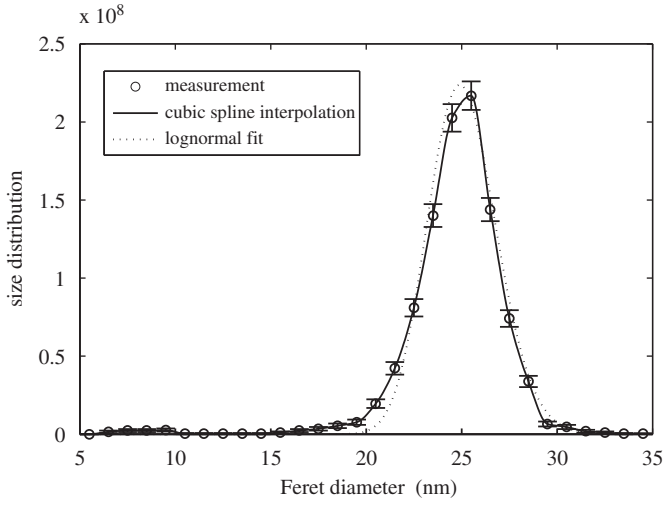

Fig. 2. Normalized probability distribution function $w(D)$, based on TEM measurements on 2602 particles. A cubic spline interpolates between the measured points for both the susceptibility and relaxometry. A lognormal fit is also shown.

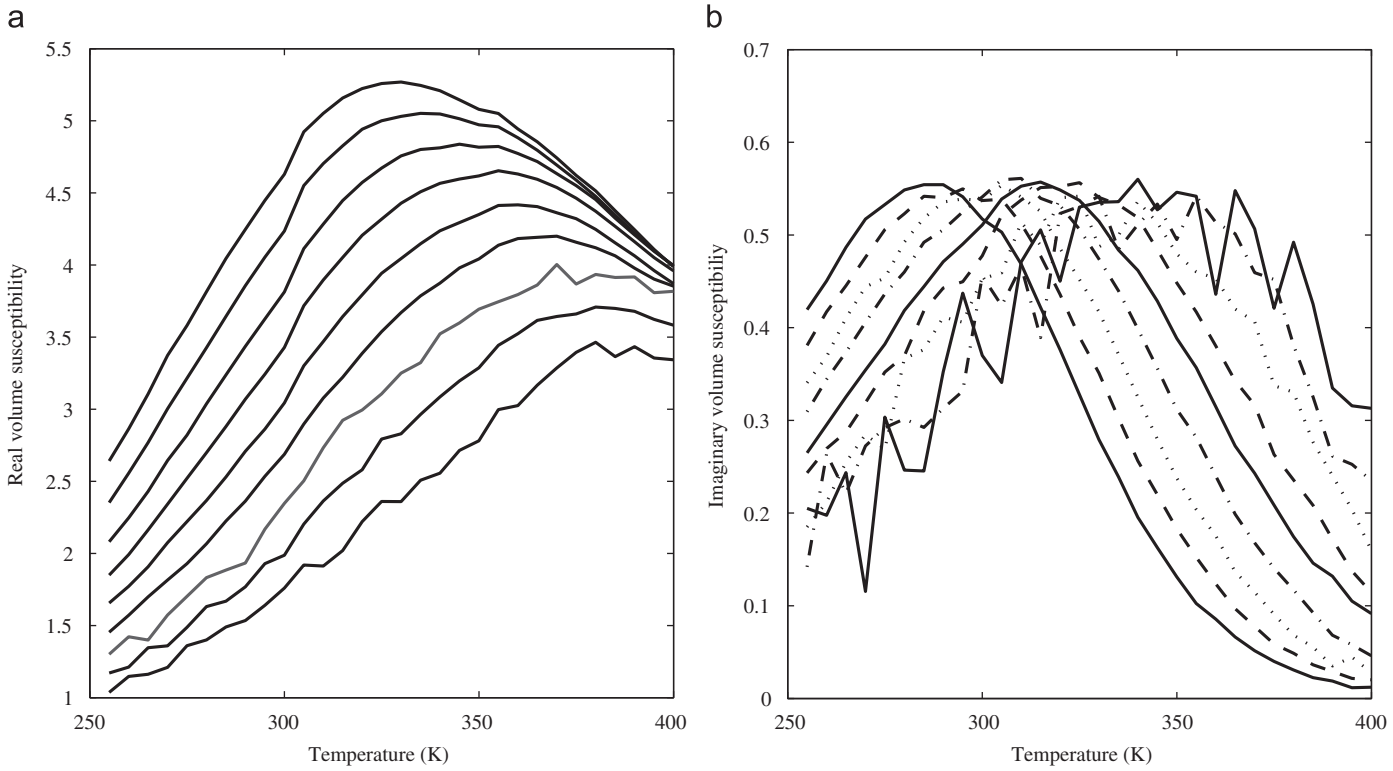

Fig. 3. Measured susceptibilities on curves of constant frequency, from top down on left: 0.1, 0.3, 1.0, 3, 10, 30, 100, 300 and 1000 Hz. The measurements are 5 K apart and joined by straight lines. The ordinates are volume susceptible in rationalized MKS. (a) Real part and (b) imaginary part.

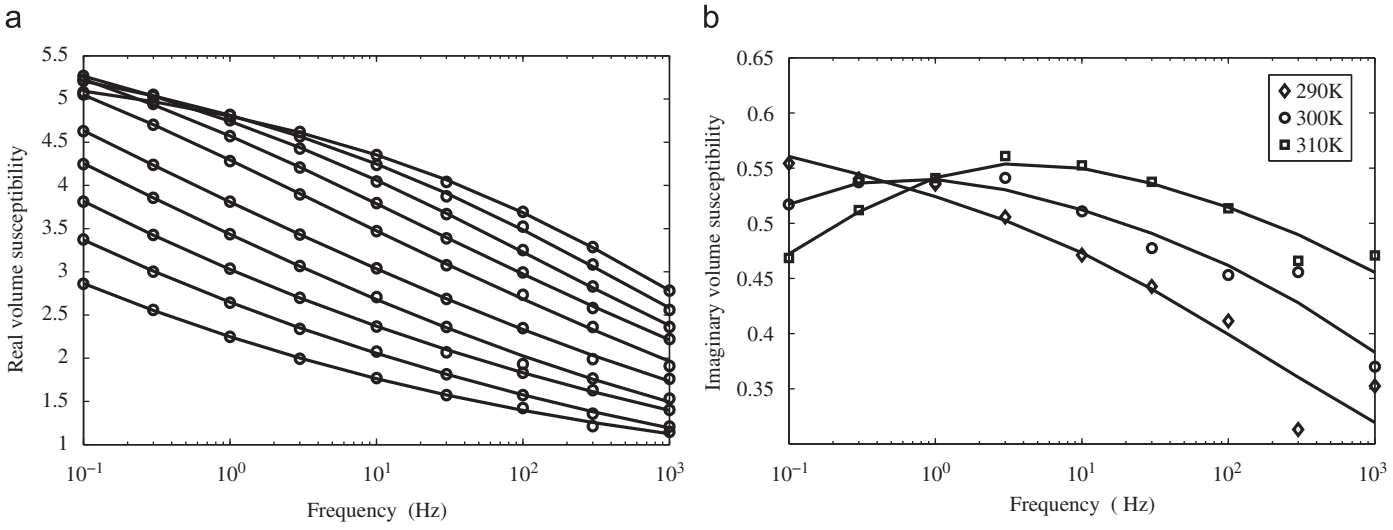

Fig. 4. Representative samples of fitted constant temperature curves for susceptibility. The 3 parameters in the model, M_s, K and τ_0, are adjusted for each temperature to give the best fit to the 9 frequency points. (a) Real part for temperatures starting right bottom up: 260–350 K in 10 K increments. (b) Imaginary part for 290 K, diamonds, 300 K, circles and 310 K, squares. There is relatively more noise in the imaginary than the real measurements because the signals are an order of magnitude smaller. All 30 constant T data sets were fit in this manner.

be compared for consistency. Each 3-paramenter curve fit contained 9 data points corresponding to the 9 frequencies. The numerical work was done using Matlab, and representative samples are shown in Fig. 4a and b.

4.4. Anatomy of susceptibility

Representative kernels contributing to the model computation are examined to see where each value arises in the nanoparticle distribution. By "kernel" we refer to the frequency-dependent integrand at a given temperature of Eq. (5) or (6) for the real or imaginary part, respectively. To compute these functions of D we use the parameters obtained by making a best fit to the data at each temperature.

As T decreases, the cluster of kernels for each T moves progressively toward the small diameter side of the distribution. For the real parts each kernel extends down to the smallest diameters, whereas for the imaginary parts each kernel is confined to a rather narrow range of sizes. Thus, for the real part, the

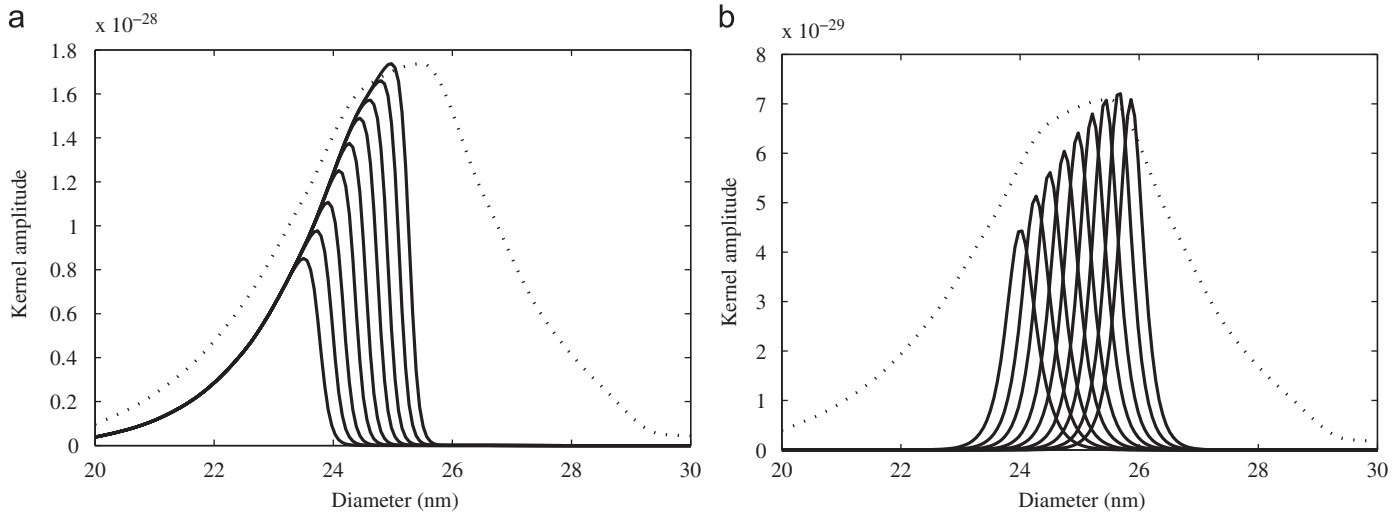

Fig. 5. Kernel functions, from Eqs. (5) and (6), at $T=300$ K, solid, and the size distribution function, dotted, arbitrary and vertical scales. The highest frequency, 1000 Hz, envelope is on the left, and the lowest, 0.1 Hz, is on the right. Similar clusters of kernels for higher (lower) temperatures correspond to larger (smaller) particle sizes. (a) Real part. (b) Imaginary part. Here each kernel probes only a narrow band in the size spectrum, in contrast with the much broader sensitivity for the real parts.

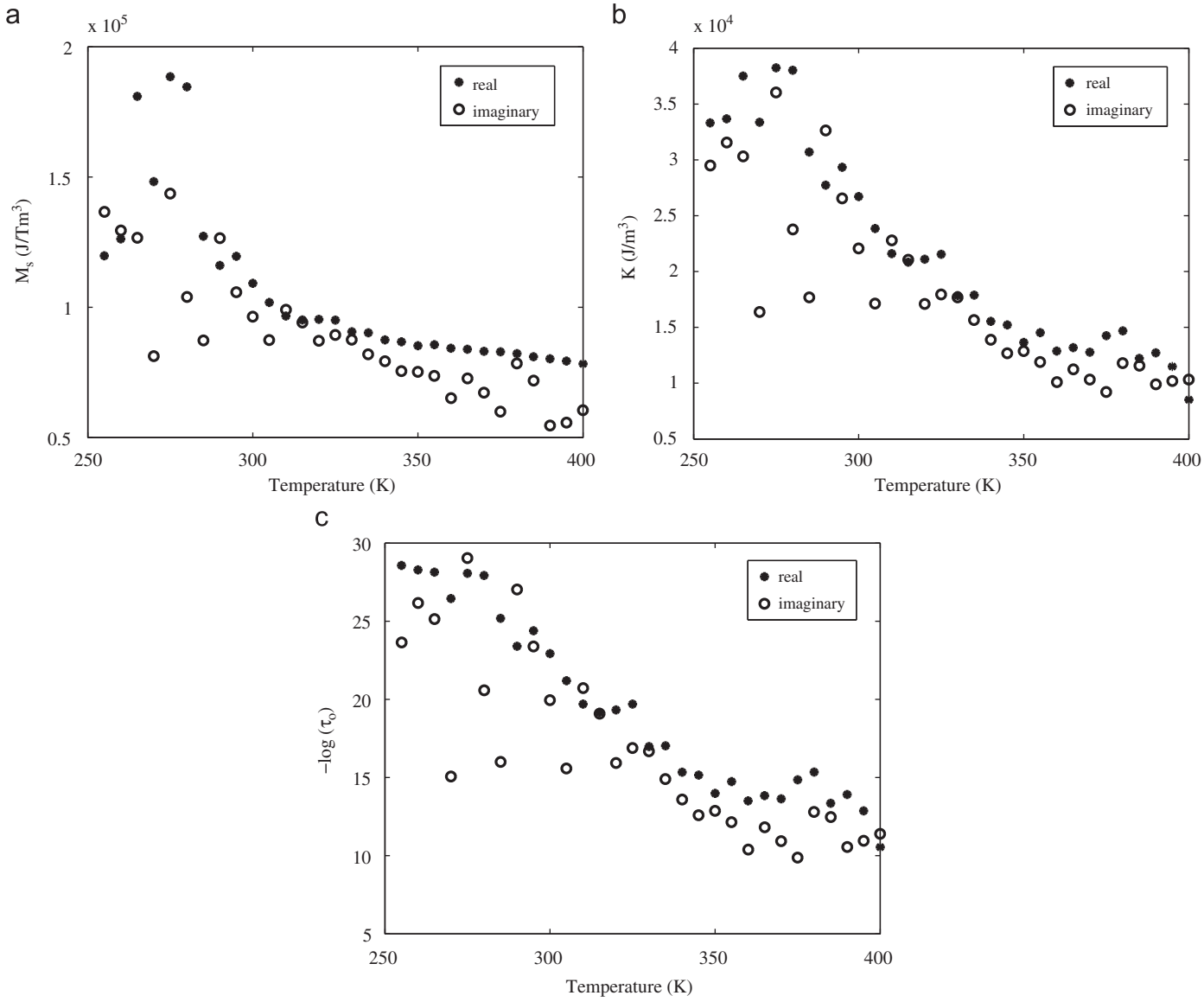

Fig. 6. Best fitted values of the three parameters vs. temperature. (a) Saturated magnetization M_s, (b) anisotropy energy density K and (c) power$=-\log\tau_0$.

$T=400$ K measurement is sensitive to the entire distribution, and the $T=255$ K cluster is influenced only by the small diameter particles. We would therefore expect results in the low temperature regions for the real part to be less robust than for the high temperature regions since the modeling is patterned by only the lower wing of the distribution, where the statistics are relatively poor. The kernels constituting the imaginary fits will also reflect poor statistics on the small side of the size distribution. In fact, our fits for both real and imaginary parts do show increasing fluctuations below 300 K (Fig. 5).

4.5. Fitted parameters

The susceptibility model (Eqs. (5) and (6)) is compared with the measured values at the nine frequencies for each temperature and the parameters M_s, K and τ_0 are adjusted to give the best fit to these data points. As the three parameters are assumed to be temperature dependent, the fit at each temperature is made independent of any other. Any size dependence of these parameters has been ignored.

Fig. 6 presents the resulting estimates for the three parameters used in our model. In all three cases the parameters determined from the real and imaginary susceptibilities are much more consistent with each other for temperatures above 300 K than for those below.

4.6. Correlation between K and log τ_0

Although the variabilities of the fitted parameters K and $\log \tau_0$ shown in Fig. 6b and c are large, the correlation between the variations is strong. Fig. 7a shows that there is an abrupt threshold just above 10 for $-\log \tau_0$. For T greater than about 300 K the ratio of these two parameters agrees well for the real and imaginary contributions.

In SQUID relaxometry applications (Section 5) the size range of nanoparticles should correspond to a relaxation time of about 1 s. In this case $\log \tau \approx 0$, allowing us via Eq. (1) to find the effective particle diameter (see discussion following Eq. (1) in Chantrell et al. [3]),

$$D_{eff} \approx (-6kT \log \tau_0 \ln 10/\pi K)^{1/3}. \quad (11)$$

Consequently, it is the ratio that determines the required diameter for SQUID relaxometry, the SQUID window, an example of which we discuss in Section 5 (see Fig. 7b).

4.7. Closer look at the fits at 300 K

We examine more closely the fits to the susceptibility data at 300 K, the temperature region of interest in biomedical applications. At this temperature our best fits correspond to a K of 2.67×10^4 and 2.21×10^4 J/m^3 for real and imaginary, respectively, which are about twice that of the bulk value of magnetite, 1.35×10^4 J/m^3. The accompanying fit for the log of τ_0, usually taken as -10, yields -22.9 and -20.0, giving a ratio $-K/\log \tau_0$ of 1.17×10^3 and 1.11×10^4 J/m^3, respectively, that, when multiplied by 10, would be well within the usually accepted range for K. In spite of the strong correlation between $\log \tau_0$ and K, we cannot simply 'renormalize' $\log \tau_0$ back to -10, however, since in this case the fit to the data is much worse. The rms difference between the model and the measurements (dimensionless) at 300 K is 0.057, and the average over all T is 0.062 with a standard deviation of 0.024. In Section 5 we use these parameters to successfully fit relaxometry data taken on the same sample.

If we use τ_n instead of τ_{10}, set $S_2=1$, and rerun the real part fit at 300 K, we get somewhat different values for the parameters ($-\log \tau_0$ increases by about 7%), but the goodness of fit is essentially unchanged.

5. SQUID relaxometry measurements

5.1. Experimental method

Here we apply the model discussed above (Section 3.4), as well as the susceptibility results (Sections 4.5 and 4.7), to the understanding of measurements done on the same Ocean 30 DE4G nanoparticles in SQUID relaxometry. The sample was the same cotton swab as used in the susceptibility measurements. For these observations the sample is subjected to pulsed magnetic fields ranging in strength up to 4 mT. The pulsed fields rise abruptly to a constant amplitude and are terminated abruptly after a fixed duration, with a quench time of a few ms. Data collection begins when the lingering effects of the applied pulsed field and associated transients are essentially undetectable, 50 ms past the switch-off, by a SQUID array above the sample. The sample and the SQUID array lie along the axis of a Helmholtz pair, with the sample

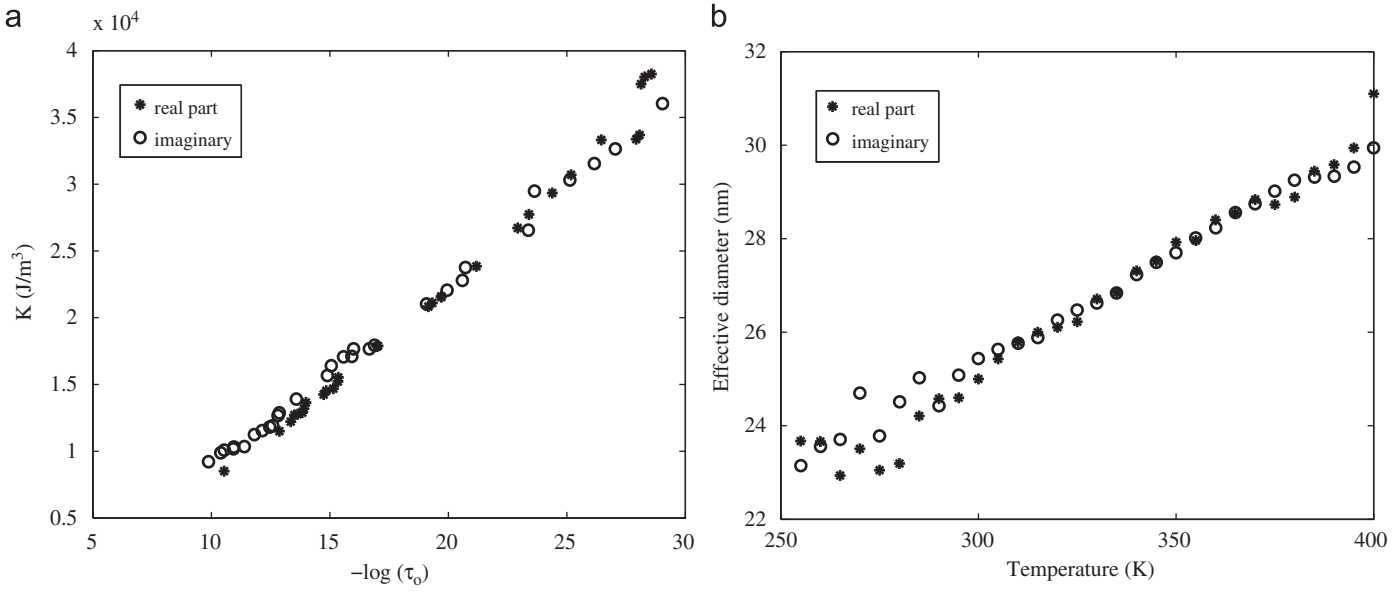

Fig. 7. Correlations (a) K vs. $\log \tau_0$. Note that the data indicate an abrupt threshold of $-\log \tau_0$ at 10. (b) The effective diameter, D_{eff}, which depends on K over $\log \tau_0$, corresponds to a time constant of 1 s.

centered between the two coils. The apparatus is described in more detail elsewhere [4,5].

We compare the relaxation of the induced moment of the sample after field switch-off with the model predictions for three applied pulse durations, 0.3, 0.75 and 1.5 s. We also examine the excitation curves for the three cases, namely, the induced moment (50 ms after the pulse is switched off) as a function of pulsed field strength.

The two sets of data, consisting of three curves each, can be modeled with Eq. (9). In the decay case we have the magnetic field produced by the decaying magnetic moment from the particles as measured by the SQUID array, $B_s(t)$, vs. time, ranging up to 2 s after the pulse is switched off, and, in the excitation case, we have the magnetic moment of the sample $M(t)$ at $t=50$ ms (after the field is switched off) vs. the strength of the pulsed field.

5.2. The model

To model these data we use the cubic spline fit to the size distribution $w(D)$ for the Ocean SHP 30 DE4G sample (Fig. 2) discussed above. We define the "SQUID window" as the size range of a particular lot of nanoparticles for which the time constants will allow the SQUIDs to pick up a measurable signal from the relaxation of the particles after the alignment pulse is switched off (Fig.7b). The amplitude for the maximum signal we can expect with the above-described apparatus is proportional to

$$f(D) = vwg(t_p)L(\sigma,\xi)\exp(-50\,ms/\tau). \tag{12}$$

The initial induced moment from a sample of n particles is

$$M(t=50\,\text{ms}) = nM_s\int_0^\infty f(D)dD. \tag{13}$$

Table 1
Fraction of sample moment observed by relaxometry.

Pulse duration seconds (t_p)	Fraction SQUID-visible
0.3	0.020
0.75	0.025
1.5	0.028

The total magnetic moment of the sample is

$$M_{sample} = nM_s\int_0^\infty vwdD. \tag{14}$$

The fraction of magnetic moment that will be SQUID-visible is then just the ratio of these two quantities for the largest pulsed field amplitude used in the excitation measurements (see Table 1).

5.3. Results

Fig. 8 presents the SQUID measurements of (a) relaxation and (b) excitation of the sample of magnetite nanoparticles for three different pulse durations compared with the model results, using parameters determined for 300 K. The model data shown are plotted for $\alpha=3/2$. This value appears optimal for Fig. 8b, but for Fig. 8a the optimal value is near $\alpha=2$. The model predictions were normalized by one fitted constant for Fig. 8a and one for Fig. 8b. As mentioned in Section 4.7, the introduction of Eq. (8) does not affect the overall goodness of fit. It does, however, increase the most favorable diameter from around 25 to 26.5 nm.

5.4. Determination of the number of particles

The model moment prediction for the single nanoparticle, $y=M_s\int_0^\infty f(D)d\text{D}$, produces a model data set, y_i, for a set of pulsed fields and pulse durations. The measured data set corresponding to the model set is d_i. The predicted value for d_i is ny_i, where n is the number of particles. A least squares fit yields

$$n = \sum_i y_i^2 / \sum_i d_i y_i. \tag{15}$$

For the data and the models to which they are compared in Fig. 8b, we find $n=1.9\times10^{13}$. Earlier to this sample, a cotton tip, on which fluid containing the suspended particles had been allowed to evaporate, was estimated (Section 4.2) to contain 9.4×10^{12} particles.

6. Conclusion

We have been able to model the response of a sample of nanoparticles to an AC susceptometry measurement and, fitting the model to the observation, extract values as a function of temperature of three parameters important to understanding the magnetic behavior, M_S, K and $\log\tau_0$. In the same spirit, with the values of the

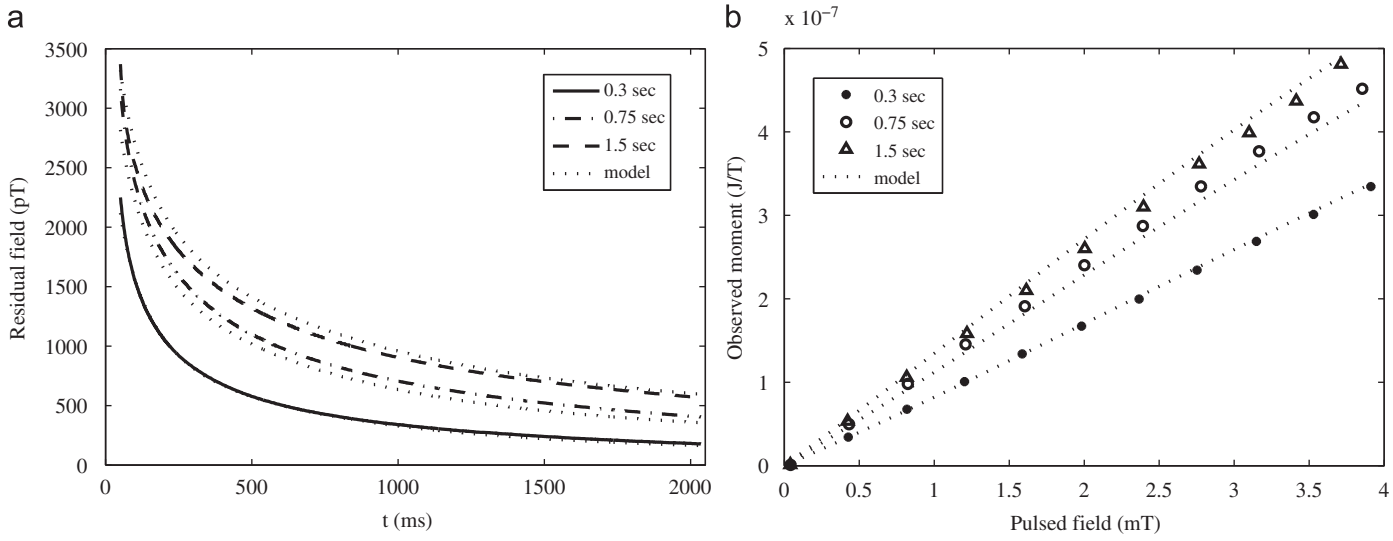

Fig. 8. SQUID relaxometry model (dotted line) compared with measurements for the three pulse durations. (a) Relaxation and (b) excitation.

parameters extracted from the susceptibility measurements, we fit results of a SQUID relaxometry study of the same sample of particles at 300 K for three pulse durations. We have introduced a modified Langevin function to include the influence of K on the equilibrium alignment of the moment of a constrained particle with the applied field. Although the use of this semiempirical approach produces reasonable fits to the data, understanding the interplay between rather large values of K and the extremely low, seemingly unphysical, values of τ_0 requires further study.

Acknowledgements

Thanks to James R. O'Brien of Quantum Design and Andrew Wang and John Dixon of Ocean Nanotech for their help and kind advice. Thanks also to Richard Larson, Kimberly Butler and Maureen Flynn for their interest and support. Comments from Sara Majetich were very useful. Comments from an anonymous referee substantially improved this paper.

Senior Scientific, LLC, acknowledges the support of the National Institutes of Health under Grants R44AI066765, R44CA096154, R44CA105742 and R44CA123785. This work was performed, in part, at the Center for Integrated Nanotechnologies, a US Department of Energy and Office of Basic Energy Sciences user facility. Sandia National Laboratories is a multi-program laboratory operated by Sandia Corporation, a Lockheed-Martin Company, for the US Department of Energy under Contract no. DE-AC04-94AL85000. Natalie Adolphi acknowledges equity interests in nanoMR and ABQMR; nanoMR and ABQMR did not sponsor this research.

References

[1] W. Weitschies, R. Koetitz, T. Bunte, L. Trahms, Pharm. Pharmacol. Lett. 7 (1997) 1–4.
[2] L. Néel, Adv. Phys 4 (1955) 191.
[3] R.W. Chantrell, N. Walmsley, J. Gore, M. Maylin, Phys. Rev. B 63 (2000) 024410-1–024410-14.
[4] N.L. Adolphi, D.L. Huber, J.E. Jaetao, H.C. Bryant, D.M. Lavato, D.L. Fegan, E.L. Venturini, T.C. Monson, T.E. Tessier, H.J. Hathaway, C. Bergemann, R.S. Larson, E.R. Flynn, J. Magn. Magn. Mater. 321 (2009) 1459–1464.
[5] E.R. Flynn, H.C. Bryant, Phys. Med. Biol. 50 (2005) 1273–1293.
[6] Amikam Aharoni, Introduction to the Theory of Ferromagnetism, Oxford, 1996.
[7] W. Williams, A.R. Muxworthy, G.A. Paterson, J. Geophys. Res 111 (B12S13) (2006) 1–9.
[8] Ricardo Aragón, Phys Rev B 46 (1992) 5334–5338.
[9] S.A. Majetich, M. Sachen, J. Phys. D 39 (2006) R407–R422.
[10] R.H. Victora, Phys. Rev. Lett. 63 (1989) 457–460.
[11] Yu.L. Raikher, J. Magn. Magn. Matter 39 (1983) 11–13.
[12] Yu.L. Raikher, V.I. Stepanov, Phys. Rev. B 55 (1997) 15005–15017.
[13] I. Yasumori, D. Reinen, P.W Selwood, J. Appl. Phys. 34 (1963) 3544–3549 (Eq. (13)).
[14] F. Bentivegna, J. Ferré, M. Nývlt, J.P. Jamet, D. Imhof, M Canva, A. Brun, P. Veillet, Š. Višňovský, F. Chaput, J.P. Boilot, J. Appl. Phys. 83 (1998) 7776–7788.
[15] L. Bessais, L. Ben Jaffel, J.L. Dormann, Phys. Rev. B 45 (1992) 7805–7815.
[16] R.W. Chantrell, S.R. Hoon, B.K. Tanner, J. Magn. Magn. Matter 38 (1983) 133–141.
[17] D. Eberbeck, S. Hartwig, U. Steinhoff, L. Trahms, Magnetohydrodynamics 39 (2003) 77–83.
[18] F. Ludwig, E. Heim, M. Schilling, J. Appl. Phys 101 (2007) 113909-1–113909-10.